Title

Controllable multicompartment morphologies from cooperative self-assembly of copolymer–copolymer blends

Journal

Soft Matter, 13(35)

ISSN

1744-683X

Authors

Wang, Zhikun
Sun, Shuangqing
Li, Chunling
et al.

Publication Date

2017-09-13

DOI

10.1039/c7sm01194f

Peer reviewed

Controllable multicompartment morphologies from cooperative self-assembly of copolymer-copolymer blends[a†]

Zhikun Wang[a,b], Shuangqing Sun[a,c], Chunling Li[a,c], Songqing Hu[a,c*], Roland Faller[b*]

Abstract

Multicompartment nanostructures, such as microcapsules with clearly separated shell and core, are not easily accessible by conventional block copolymer self-assembly. We assess a versatile computational strategy through cooperative assembly of diblock copolymer blends to generate spherical and cylindrical compartmentalized micelles with intricate structures and morphologies. The co-assembly strategy combines the advantages of polymer blending and incompatibility-induced phase separation. Following this strategy, various nanoassemblies of pure AB, binary AB/AC and ternary AB/AC/AD systems such as compartmentalized micelles with sponge-like, Janus, capsule-like and onion-like morphologies can be obtained. The formation and structural adjustment of microcapsule micelles, in which the shell or core can be occupied by either pure or mixed diblock copolymers, were explored. The mechanism involving the separation of shell and core copolymers is attributed to the stretching force differences of copolymers which drive the arrangement of different copolymers in a pathway to minimize the total interfacial energy. Moreover, by adjusting block interactions, an efficient approach is exhibited for regulating the shell or core composition and morphology in microcapsule micelles, such as the transition from the “pure shell/mixed core” morphology to the “mixed shell/pure core” morphology in the AB/AC/AD micelle. This mesoscale simulation study identifies the key factors governing co-assembly of diblock copolymer blends and provides bottom-up insights towards the design and optimization of new

a† Electronic Supplementary Information (ESI) available. See DOI: XXXXXXXXX.

aa College of Science, China University of Petroleum (East China), 266580 Qingdao, Shandong, China. E-mail: songqinghu@upc.edu.cn

bb Department of Chemical Engineering, UC Davis, 95616 Davis, California, USA. E-mail: rfaller@ucdavis.edu

cc Key Laboratory of New Energy Physics & Materials Science in Universities of Shandong, China University of Petroleum (East China), 266580 Qingdao, Shandong, China.

multicompartment micelles.

1 Introduction

The development of nanotechnology makes it necessary to manipulate materials at the nanometer level, thus, the ability to control the formation of specific structures is of great interest. However, it is often experimentally tedious to determine the parameter ranges of formation and stability of certain morphologies. Computer simulations can more efficiently scan large parameter spaces and guide experimental efforts to promising areas. Amphiphilic block copolymers of two or more chemically distinct polymer blocks are an important class of self-organizing molecules and can be used as templating materials for nanodevices since they self-assemble into a variety of organized aggregates, which include, e.g., spherical[1-4], cylindrical[5-8], vesicular[9-11] and helical[12,13] nanoobjects. The parameters which govern the morphologies of these aggregates include the stretching degree of the core-forming blocks, the micelle/solvent interfacial tension and the repulsive interactions among corona-forming chains[14-16]. Morphologies can therefore be controlled by affecting contributions, such as selectivity of solvent, copolymer composition and concentration, additives, etc[14-16]. Preparation of nanoobjects with well-defined geometries, e.g., multicompartment nanoparticle assemblies with multiple internal or external subdomains, is of broad interest in nanotechnology[17-20]. Such nanoassemblies hold great promise for advanced nanotechnological applications, e.g., drug delivery, optical and electrical materials, since they represent a significant progress toward hierarchical self-assembly with versatile functions or architectural features[17-20].

Compartmentalized micelles self-assemble from pure diblock[21], triblock[1], star[8] or comb[22]

copolymers. Such structures can also be obtained from the cooperative self-assembly of block copolymer blends, such as AB/B[23-26], AB/AC[27-30], AB/CB[12,31-37] and AB/BAB[38,39]. Such structures are the focus of the study here. Capital letters represent a block of monomers of the same chemistry/interactions. The second component, which has specific interactions with either block, will increase the complexity of self-assembly and introduce a second level of hierarchy controlled by block-block interaction in addition to the solvent-block interaction[40]. Multifunctional hybrid micelles can be achieved by controlling the intermolecular self-assembly strategies including monomer selection, architecture design, solution conditions (pH, temperature, ionic strength), etc[8,41-46]. This approach represents a powerful and straightforward way to systematically tune the resulting micellar structures without having to synthesize even more complex multiblock copolymers[18]. Concentric core-shell corona[34,35] and nonconcentric[47] nanostructures have been obtained by this approach. Zhu et al.[37] produced worm-like micelles with separated cores from blends of AB copolymer, PS-b-PEO, with various hydrophobic BC copolymers, PS-b-P4VP, PS-b-PI and PS-b-PB. Gao et al.[38] obtained highly compartmentalized vesicles, multilayer and bicontinuous nanoassemblies as well as porous nanospheres from blends of AB/BAB block copolymers (PEG-b-PS/PS-b-PEG-b-PS) by combining blending and polymerization-induced self-assembly.

A cone-column mechanism involving curvature stabilization has been proposed for morphological transitions of block copolymers[48,49]. An example of this mechanism was the co-assembly of PS-b-PAA and PS-b-P4VP blends, demonstrating the preferential separation of short hydrophilic corona chains, PS-b-PAA, to the interior of the micelles and of the long chains, PS-b-P4VP, to the exterior, leading to stable interface curvature[48]. The separation was

also observed when P4VP is positively charged (which implies a stronger repulsion) while PAA chains were neutral[48]. The thermodynamic stabilization of curvatures in various morphologies is attributed to the interfacial energy between different blocks (enthalpy) and the stretching of copolymers (entropy)[14]. Thus, the central challenge for the formation of multicompartment micelles from block copolymer blends lies in directing multiple non-covalently linked and immiscible phases into different subdomains, in such a way as to minimize the total interfacial energy[14]. Our study will focus on the parameter space where the different morphologies form and are stable.

To date, most studies involving the co-assembly of block copolymer blends have focused on the synthesis of polymers with particular chain architecture and electrostatic interaction[18,50], which, as indicated in the cone-column mechanism, provide a specific driving force for phase separation. These two aspects are mainly related to the intra- (relating to chain stretching) and inter- (relating to block incompatibility) repulsions of block copolymers. However, due to the complexity of coexisting mixed micelles from architecturally and chemically versatile block copolymers[14,18,50,51], many more explorations are needed.

The present work extends previous studies by systematically exploring the morphological consequences of changes in intra- and inter-repulsion strengths in block copolymer blends. Even a slight change in environmental conditions (e.g., pH, temperature) can have a major effect on the micellar morphology[34,35]. Experimentally, modification of the repulsions can be realized by adopting stimuli-responsive block copolymer[52], in-situ reaction of copolymers[53], or modifying solution parameters[29]. A systematic variation in the intra- and inter-repulsions of block copolymer blends will lead to better understanding of the co-assembly mechanism of

novel nanoassemblies.

Here, we explore the self-assembly of three types of systems, pure AB copolymers, binary mixtures AB/AC and ternary mixtures of AB/AC/AD copolymers, in which block A is hydrophilic and blocks B, C and D are different but all hydrophobic. The three diblock copolymers have to limit the already vast parameter space a symmetric chain architecture (equal monomer number per block) and equal chain length. The solvent selectivity of blocks B, C and D were kept the same to avoid interface driven arrangements. Two typical shapes of micelles, spheres and cylinders, were considered. The diblock copolymers in these systems were controllably guided into specific assembly pathways through the co-assembly of different copolymers, and the resulting nanostructures are, at least, kinetically stable. The role of chain stretching and block repulsion in the morphology transition and the formation mechanism was studied. Many multicompartment morphologies with precisely controlled core or shell composition and structure were obtained, and the strategy for the preparation of such structures was revealed.

2 Computational methods

We use dissipative particle dynamics (DPD)[54], a coarse-grained simulation technique that employs a soft repulsive potential and a momentum-conserving thermostat to control interactions of beads representing clusters of molecules. As a mesoscale method, DPD can be used to study physical phenomena at larger time and spatial scales than typical molecular dynamics. It has been successfully used for determining the mesophase self-assembly of block copolymers with various chain architectures[11,55].

In DPD, the many-body system evolves under Newton's second law $m\, d\boldsymbol{v}_i/dt = \boldsymbol{f}_i$, where

$\boldsymbol{v}_i$ and $\boldsymbol{f}_i$ denote the velocity and force on the ith bead with mass m at time t. The equation of motion is integrated using the velocity-Verlet algorithm[54]. The force on bead i is a sum of a conservative, dissipative, and random forces as well as bond stretching force, i.e., $\boldsymbol{f}_i = \Sigma_j (\boldsymbol{F}_{ij}^C + \boldsymbol{F}_{ij}^D + \boldsymbol{F}_{ij}^R) + \boldsymbol{F}_{ij}^S$, where the sum runs over all beads j within a cutoff radius r_c. The conservative force is given by $\boldsymbol{F}_{ij}^C = a_{ij}\omega^C(r_{ij})\boldsymbol{e}_{ij}$, where a_{ij} is the maximum repulsive parameter between beads i and j. The weight function is $\omega^C(r_{ij}) = 1 - r_{ij}/r_c$ for $r_{ij} < r_c$ and $\omega^C(r_{ij}) = 0$ for $r_{ij} \geq r_c$. The dissipative and random forces are $\boldsymbol{F}_{ij}^D = -\gamma\omega^D(r_{ij})(\hat{\boldsymbol{r}}_{ij} \cdot \boldsymbol{v}_{ij})\hat{\boldsymbol{r}}_{ij}$ and $\boldsymbol{F}_{ij}^R = \sigma\omega^R(r_{ij})\xi_{ij}(dt)^{1/2}\hat{\boldsymbol{r}}_{ij}$, respectively, where $\hat{\boldsymbol{r}}_{ij} = \boldsymbol{r}_{ij}/r_{ij}$ with $r_{ij} = |r_i - r_j|$, $\boldsymbol{v}_{ij} = \boldsymbol{v}_i - \boldsymbol{v}_j$, and ξ_{ij} is a zero-mean Gaussian random variable of unit variance with $\xi_{ij} = \xi_{ji}$. Both, dissipative and random, forces act together as a thermostat of the system. Their strengths are determined by γ and $\sigma^2 = 2k_BT\gamma$, respectively, where k_B is the Boltzmann constant and T is the system temperature. The bond stretching force is represented by $\boldsymbol{F}_{ij}^S = C\boldsymbol{r}_{ij}$ with a stiffness constant C. We use the dissipative parameter $\gamma = 4.5$, thermal energy $k_BT = 1$ and stiffness constant $C = -4$.

The repulsive parameter a_{ij} determines interactions of polymer blocks. By assuming $a_{ii} = a_{jj}$, a_{ij} is determined by the Flory-Huggins parameter χ_{ij} through[54] $a_{ij} = a_{ii} + 3.50\chi_{ij}$. The χ_{ij} among polymer blocks can be obtained from $\chi_{ij} = (\Delta E^{mix}V_r)/(RT\phi_i\phi_jV)$, where R is the gas constant and T is temperature; ϕ_i and ϕ_j are the relative fractions of components i and j; V is total volume and V_r is the reference volume; ΔE^{mix} is the mixing energy of two components. One can use a typical diblock copolymer, PS (polystyrene)-b-PEO (polyethyleneoxide), as reference to relate to experiments. The repulsive parameters of water-PS, water-PEO and PS-PEO are $a_{W\text{-}PS} = 76.18$, $a_{W\text{-}PEO} = 26.05$, $a_{PS\text{-}PEO} = 37.04$, consistent with previous studies[55-57]. The detailed simulation procedure was identical to that in Ref. [55]. The repulsive parameters of

the three typical systems, i.e., AB, AB/AC and AB/AC/AD, were mainly based on the PS-b-PEO system. All like-particle repulsive parameters were set to a_{ii} = 25, and the repulsive parameters between all hydrophobic blocks and water were identical, i.e. $a_{BW} = a_{CW} = a_{DW}$ = 76.18. In particular, water selectivity of the hydrophilic blocks was examined by varying a_{AW} from 20 to 33; self-repulsions of copolymers, i.e., the repulsive parameters between the two blocks on copolymer chains, were examined by varying a_{AB}, a_{AC} and a_{AD} from 25 to 60; compatibilities of different types of copolymers were examined by setting a_{BC}, a_{BD} and a_{CD} to 25 (compatible) or 45 (incompatible). The repulsive parameters are shown in Table 1.

Table 1. Repulsive parameters a_{ii} used in DPD simulations.

	A	B	C	D	W
A	25				
B	25~60	25			
C	25~60	25/45	25		
D	37.04/60	25/45	25/45	25	
W	20/26.05/33	76.18	76.18	76.18	25

Simulations were carried out using the LAMMPS simulation package[58]. The three types of diblock copolymer chains all have 5 hydrophilic beads of type A bonded to 5 hydrophobic beads of one of the other types B, C or D. The starting structures were constructed by randomly placing the solvent beads and polymers in a cubic box of size $45r_c \times 45r_c \times 45r_c$, containing 273,375 beads. Two typical volume fractions of polymer, 20% and 30%, were considered throughout the paper. Periodic boundary conditions were applied in all directions. The initial structures were first energy minimized for 1,000 steps using a conjugate gradient algorithm. Then, production runs started by generating random velocities on all particles by a Gaussian distribution, and use 1.5×10^6 steps for each model. If this does not lead to a stable morphology, another run of the same length is added. In our simulations, we set the time step

Δt = 0.05, bead mass m = 1, cutoff radius r_c = 1 and temperature T = 1. All values are given in DPD units.

3 Results and discussion

3.1 Self-Assembly of Pure AB Systems

For nanoassemblies of individual block copolymers, their morphology can be tuned by solvent selectivity of polymer blocks and chain stretching[14]. In the AB system with equal molar ratio of A and B, the morphology depends largely on the hydrophilicity of block A and the repulsive force between A and B. The effect of the hydrophilicity of block A on the morphology of the AB system was studied for AB concentrations (ϕ_{AB}) from 10% ~ 30% (Figure S1 in Supporting Information (SI), a_{AB} = 37.04, a_{BW} = 76.18). At a_{AW} = 20, block A is extremely hydrophilic and a set of separated worm-like clusters was obtained due to the very large micelle/solvent interface tension. The cluster number is increased by increasing ϕ_{AB}, while the cluster size is nearly unaffected. At a_{AW} = 26.05, block A is compatible with solvent and the polymers tend to form bilayer systems (vesicles at $\phi_{AB} \leq$ 15% or lamellae at $\phi_{AB} \geq$ 20%). Larger a_{AW} value at 33 leads to big aggregated micelles (spheres at $\phi_{AB} \leq$ 25% or cylinders at ϕ_{AB} = 30%) with multicompartment (sponge-like) inner structures due to the smaller micelle/solvent interface tension. The morphological evolution “from worm to bilayer to multicompartment” affords the equilibrium system reduced micelle/solvent interface area (or energy) and increased configurational entropy of copolymers[14]. The self-assemblies at a_{AW} = 26.05 are consistent with real PS-b-PEO solution in experiments[4,38,59].

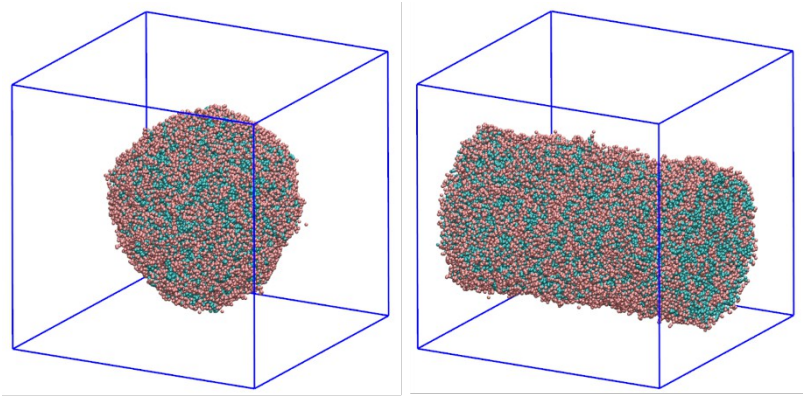

Figure 1. Morphologies of the pure AB system when ϕ_{AB} equals 20% (sphere) and 30% (cylinder) (a_{AW} = 33, a_{AB} = 37.04, a_{BW} = 76.18). Color scheme: A-pink, B-cyan. Water is not shown for clarity.

Compared to worm-like or vesicular morphologies, the spherical or cylindrical micelles a_{AW} = 33 with subdivided solvophobic cores have greater potential as multicompartment templates (Figure 1)[18]. These micelles grow in size proportionately if the box volume were increased (Figure S2 in SI). However, the box size effects are not dominating. We performed additional simulations where we doubled the system size of the 45^3 system in two directions (quadrupled volume). The micelles are complete stable at the continuation of the simulations (Figure S3 in SI). We also performed simulations with 44^3 and 46^3 system size keeping the particle number the same as in the 45^3 simulation where we again see stable simulations with slightly changed pressure again indicating that system size has only a minor effect (Figure S4 in SI).

The effect of chain stretching on the morphology of the AB system was studied focusing on the spherical and cylindrical micelles at a_{AW} = 33. As shown in Figure 2a, with increasing a_{AB} from 30 to 60, the interior structures of the two micelles grow from extremely small hydrophobic subdomains (e.g., 30) to larger hydrophobic subdomains (e.g., 37.04 and 45),

and finally to well-ordered onion-like hydrophobic subdomains (three layers). The morphological transitions were quantitatively examined by measuring the radial density profiles of block B as a function of a_{AB} (Figure 2b and 2c). In the case of the spherical micelle (Figure 2b), a plateau (r < 12) and a peak (r = 13.8) are observed at a_{AB} = 25, corresponding to the disordered sponge-like subdomains and the more aggregated surface layer, respectively. With increasing a_{AB}, two more peaks appear, and the peak height is gradually increased, indicating larger layering of the blocks at the peak positions. Finally, at a_{AB} = 60, the lowest point between two peaks reaches zero, indicating that blocks A and B are fully segregated and a perfect onion-like structure is obtained. Similar transitions can be obtained from the radial density profiles of the cylindrical micelle. Moreover, according to the highest points of the peaks at a_{AB} = 60, the layer densities of the spherical and cylindrical onions are averaged to be 3.51 and 3.37, respectively, which are about 17% and 12% larger than the system density (ρ = 3). The averaged widths between neighboring hydrophobic layers are 4.72 and 4.79 for the spherical and cylindrical micelles, respectively.

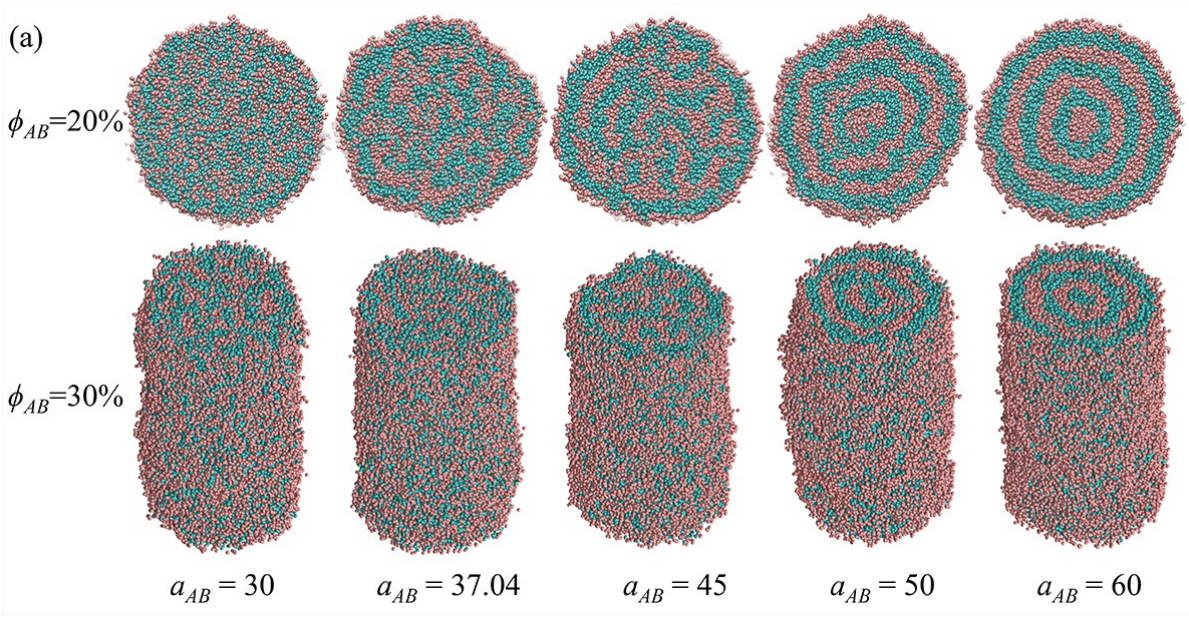

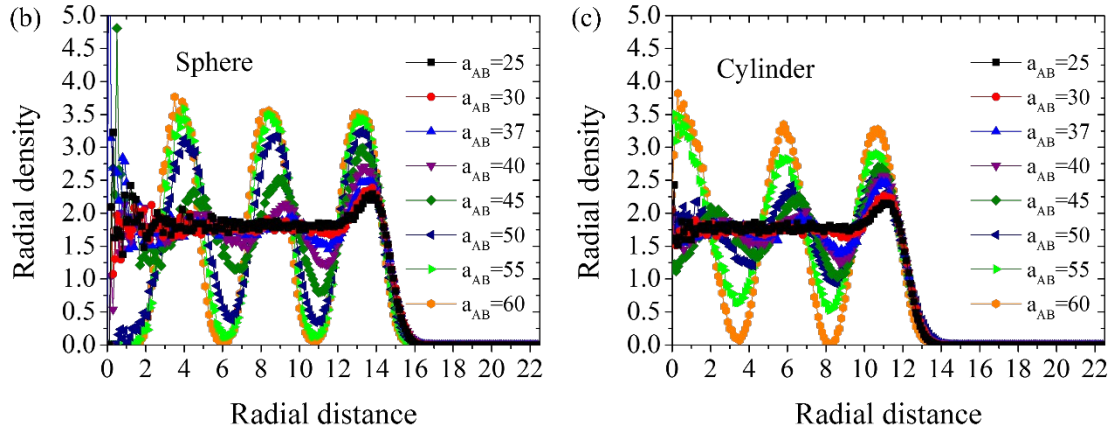

Figure 2. Morphological variations (a) and radial density (block B) profiles (b,c) of the spherical (cross sections, ϕ_{AB} = 20%) and cylindrical (ϕ_{AB} = 30%) micelles as a function of a_{AB} (a_{AW} =33, a_{BW} =76.18). Color scheme for morphologies as in Figure 1.

The formation of onion-like nanoassemblies has been experimentally observed for similar diblock copolymer systems by controlling solvent selectivity or chain stretching[2-4]. Since larger a_{AB} increases the segregation of the polymers, the two blocks separate from each other to minimize interfacial area and lower interfacial energy. The aggregated random subdomains of the two blocks prefer to adopt arrangements to align perpendicular to the normal of the micelle, leading to a morphological transition from random distribution state to concentric layered state, such as onion-like, with less curved interfaces and are energetically favorable[14]. Therefore, for AB copolymers with a proper hydrophilicity of block A (a_{AC} = 33), multicompartment spherical or cylindrical micelles with specific arrangement of hydrophobic subdomains can be obtained through controlling the repulsion of the two blocks.

3.2 Cooperative Self-Assembly of Binary AB/AC Systems

If a second solvophobic component C is included, e.g., in AB/AC blends, it is possible to access additional elaborate structures with subdivided B and C core domains[18]. In an A

selective solution, the cooperative self-assembly of the AB/AC blends depends largely on factors such as relative segregation degree of AB and AC, compatibility of B and C and relative concentration of AB and AC[14,50]. Figure 3 shows a morphology diagram obtained from AB/AC blends (20% and 30% with ϕ_{AB} : ϕ_{AC} = 10% : 10% and 15% : 15%, respectively) as a function of a_{AB} and a_{AC} when blocks B and C are compatible (a_{BC} = 25) and incompatible (a_{BC} = 45). In general, the two concentrations 20% and 30% of the blends lead to spherical and cylindrical morphologies, respectively. When B and C are miscible (a_{BC} = 25), the two blended blocks form sponge-like (or porous) hydrophobic domains within the micelle at small values of a_{AB} and a_{AC}, and with increasing a_{AB} and/or a_{AC}, the hydrophobic domains gradually become well-ordered onion-like due to increased segregation of copolymers. Examples for a_{AB}/a_{AC} 37.04/37.04, 60/37.04 and 60/60 are presented. For larger incompatibility of B and C (a_{BC} = 45), the two subdomains are completely separated due to strong repulsion. Janus-like morphologies where multiple B and C domains each occupy half of the micelle, are obtained at segregation degrees of a_{AB} = a_{AC} = 25 ~ 40 (e.g., a_{AB} = a_{AC} = 37.04). If a_{AB} is larger than a_{AC} (e.g., a_{AB} = 60, a_{AC} = 37.04), AB copolymers are driven to the surface of the micelle, while AC copolymers become encapsulated. The encapsulation happens only if AC cannot form well-ordered layering structures. If a_{AC} also becomes very large (e.g., a_{AB} = a_{AC} = 60), both copolymers have strong segregation and form onion-like layers in the micelle, and as a result, the onion-like layers are randomly occupied by separated B and C domains due to the competing alignment of them. Similar morphological evolutions are observed in both spherical (20%) and cylindrical (30%) micelles.

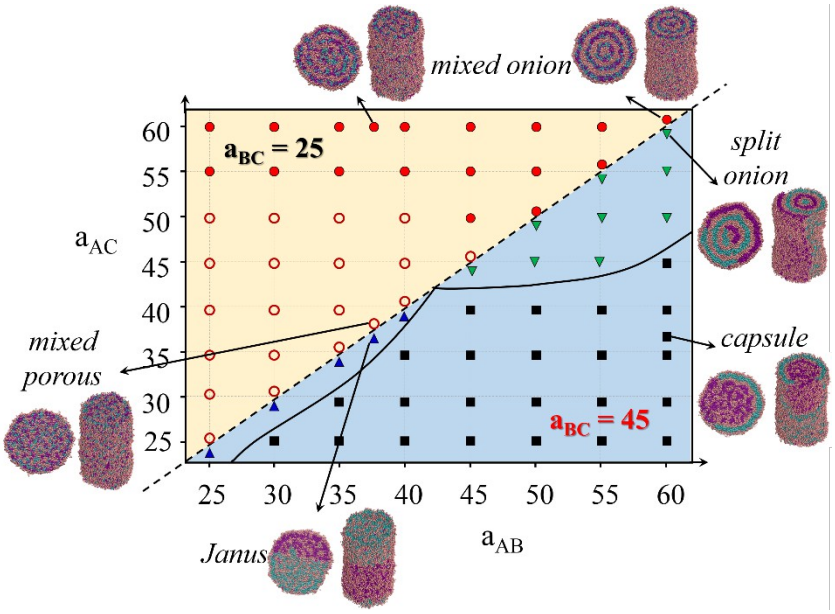

Figure 3. Morphology diagram of the spherical (cross sections, ϕ_{AB} : ϕ_{AC} = 10% : 10%) and cylindrical (ϕ_{AB} : ϕ_{AC} = 15% : 15%) micelles at different values of a_{AB} and a_{AC}. Down triangle region: a_{BC} = 25; up triangle region: a_{BC} = 45. Symbols of open circle (○), solid circle (●), solid up triangle (▲), solid down triangle (▼) and solid square (■) represent micelles with mixed porous, mixed onion, Janus, split onion and capsule morphologies, respectively. Color scheme for morphologies: A-pink, B-cyan, C-purple.

Multicompartment micelles with separated AB shell and AC core (a_{AB} = 60, a_{AC} = 37.04, a_{BC} = 45) should be dependent on the relative concentration of the two copolymers. Figure 4a shows the morphological evolutions of the spherical and cylindrical micelles as a function of ϕ_{AB} : ϕ_{AC}. Since AB copolymers prefer the surface, a growing tendency of the AB shell area is observed with increasing ϕ_{AB}. For spherical and cylindrical micelles, complete outer shells are obtained at ϕ_{AB} : ϕ_{AC} = 13% : 7% and 17.5% : 12.5%, and two complete shells are obtained at ϕ_{AB} : ϕ_{AC} = 18.7% : 1.3% and 27.5% : 2.5%, respectively. The formation of multiple shells on the micelle is outside-in as a function of ϕ_{AB}, which provides a possible strategy for controlling the local shell structure of microcapsule micelles. The encapsulation processes are

quantitatively examined by plotting the radial density profiles of block B versus ϕ_{AB} (Figure 4b and 4c). Three density peaks representing the three hydrophobic layers in the two models appear and grow with increasing ϕ_{AB}. For, both, the spherical and cylindrical micelles, the hydrophobic layer densities are measured to be 3.49 and 3.38 (highest point of peak), and the widths between neighboring hydrophobic layers are 4.82 and 4.84, respectively. The structures of the assembled microcapsules, e.g., shell number, shell thickness and core capacity, depend largely on the architecture and concentration of the copolymers. More intriguing local structures can be obtained by properly modifying the polymer or solution properties.

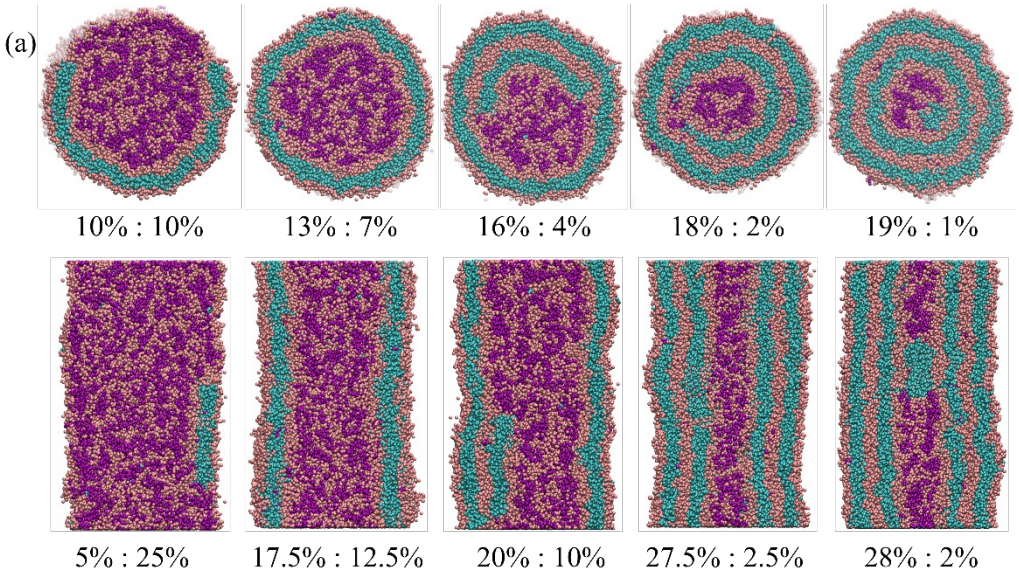

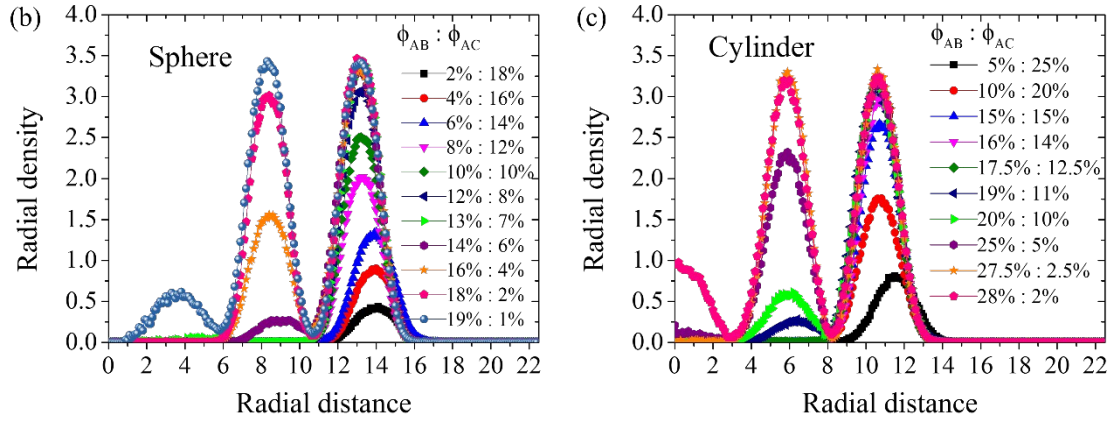

Figure 4. Morphological evolutions and radial density (block B) profiles of the spherical and cylindrical micelles as a function of ϕ_{AB} : ϕ_{AC} in the binary AB/AC systems (cross sections, a_{AB} = 60, a_{AC} = 37.04, a_{BC} = 45). Color scheme for morphologies: A-pink, B-cyan, C-purple.

Based on the observation that block copolymers with larger segregation degree form the shell of a micelle, we examined possible pathways to modify the surface properties by regulating the relative locations of AB and AC domains. The ability to regulate the surface property of nanostructures can be potentially applied to nanodevices demanding stimuli sensitive change of surface property[60]. In Figure 5, we first obtain spherical micelles with AB and AC occupying the shell and core regions, respectively (a_{AB} = 37.04 and a_{AC} = 30), then a_{AC} is increased to 60 to study the morphological evolution of the micelles. In experiments, such a property variation of copolymers can be accomplished by changing solution conditions[5,27]. Our simulations show that if the initial micelle has an incomplete AB shell (ϕ_{AB} < 13%), the increased segregation force of AC at a_{AC} = 60 will drive them to the micelle surface through the notch on AB shell, thus the relative location of AB and AC is reversed. The surface coverage of the reversed micelle depends on the initial ϕ_{AB} : ϕ_{AC} (e.g., a complete reversed shell at 7% : 13%, and an incomplete reversed shell at 10% : 10%). However, if the

initial micelle has a complete shell ($\phi_{AB} \geq 13\%$), the reversal of AB and AC does not happen at a_{AC} = 60, but the AC core orders in an onion-like structure. In this case the reversing force of AC copolymers is not large enough to break the integrity of the shell and AC copolymers are kinetically trapped.

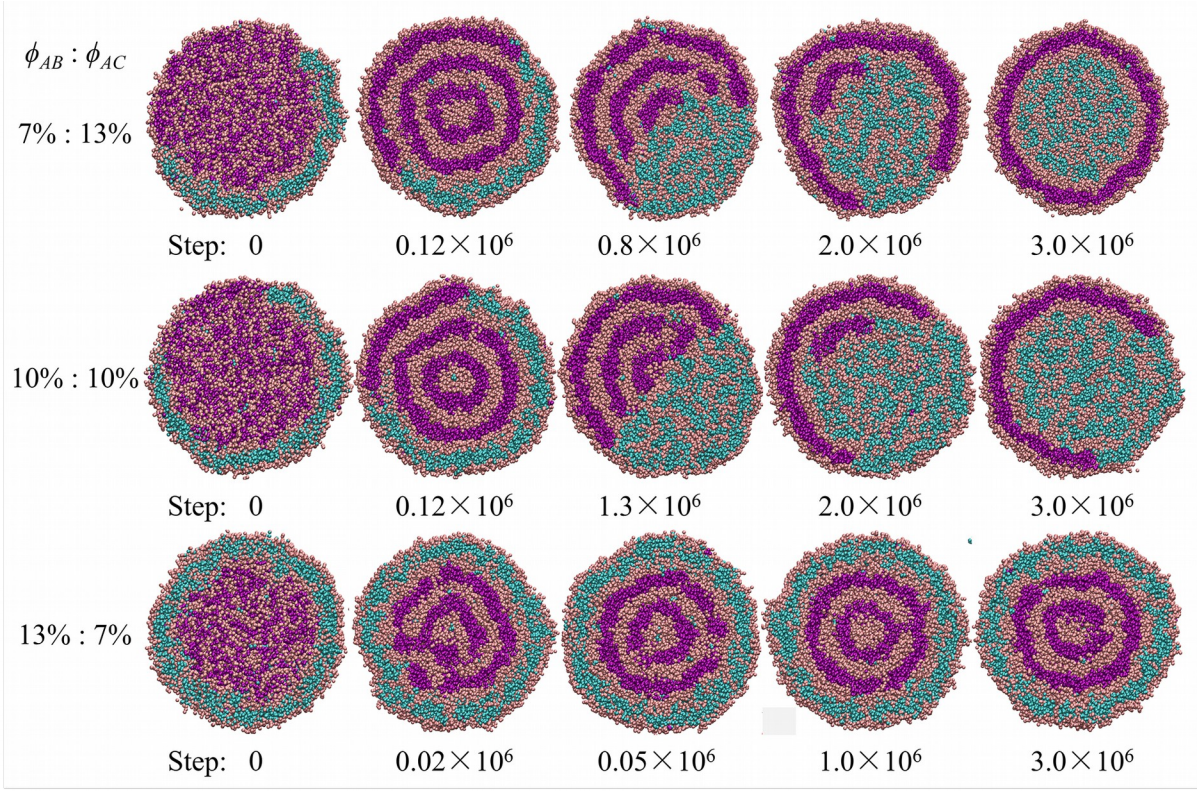

Figure 5. Reverse evolutions of the spherical micelles with several typical values of ϕ_{AB} : ϕ_{AC} when a_{AC} is increased from 30 to 60 (cross sections, a_{AB} = 37.04, a_{BC} = 45). Color scheme as in Figure 4.

It should be noted that the relative size of a_{AB} and a_{AC} should be precisely controlled to obtain perfect microcapsule structures in binary AB/AC micelles. Figure 6 presents the morphological evolutions of the spherical (ϕ_{AB} : ϕ_{AC} = 13% : 7%) and cylindrical (ϕ_{AB} : ϕ_{AC} = 17.5% : 12.5%) microcapsules with complete shells as a function of a_{AC} (a_{AB} = 60 and a_{BC} = 45). At a_{AC} = 37.04 and 45, both micelles show controllable structures in which AB and AC copolymers occupy the shell and the core regions, respectively. However, at a_{AC} = 50, 55 or

60, AC copolymers will compete with AB copolymers for their locations since they both tend to occupy the surface layer of the micelle, and the overall arrangement of the AB and AC domains becomes irregular. There appears to be a threshold for the segregation degree of AC at which AC are totally encapsulated by AB. If AC copolymers have larger segregation degree than the threshold, AB copolymers will not be able to pass though the surrounding AC layer, even though the outward driving force of AB is still larger than AC. This is instructive for the preparation of microcapsule structures with specific compositions of the shell and core that one has to be very careful about the relative size of the segregation degrees of the two diblock copolymers.

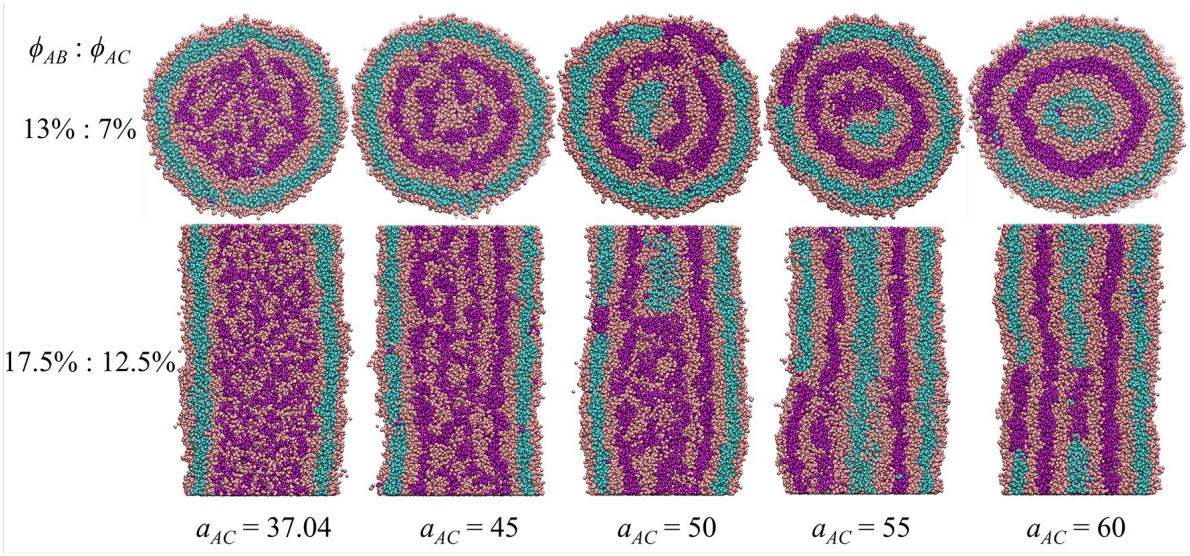

Figure 6. Morphological evolutions of the spherical and cylindrical micelles as a function of a_{AC} (cross sections, a_{AB} = 60, a_{BC} = 45). Color scheme as in Figure 4.

The morphologies of AB/AC self-assembled blends demonstrate a new way to prepare novel multicompartment micelles with precisely controlled local structures. Scheme 1 presents three co-assembly pathways based on the combination of a pure porous (sponge-like) micelle and a pure onion-like micelle, which can be obtained from diblock copolymers

with weak or strong segregation degrees, respectively. Specifically, the combination of two porous micelles (i.e., both weak segregation degrees) will lead to Janus or mixed porous micelles, the combination of a porous micelle and an onion-like micelle (i.e., weak and strong segregation degrees, respectively) will lead to capsule-like and mixed onion-like micelles, and the combination of two onion-like micelles (i.e., both strong segregation degrees) will lead to split onion-like and mixed onion-like micelles, depending on the incompatibility of two hydrophobic blocks. Clearly, two major factors, i.e., intra- (segregation degree) and inter- (incompatibility) repulsions of diblock copolymers, have profound effects on controlling the arrangement of the two polymers in the micelle. In driving polymer arrangements, the intra-repulsion provides an outside-in mechanism based on curvature (or strength) of layered copolymers, while the inter-repulsion provides a demixing mechanism based on incompatibility of hydrophobic blocks, in such a way as to minimize the total interfacial energy. The availability of diverse morphologies from diblock copolymer blends is therefore dependent on the competition of the two mechanisms.

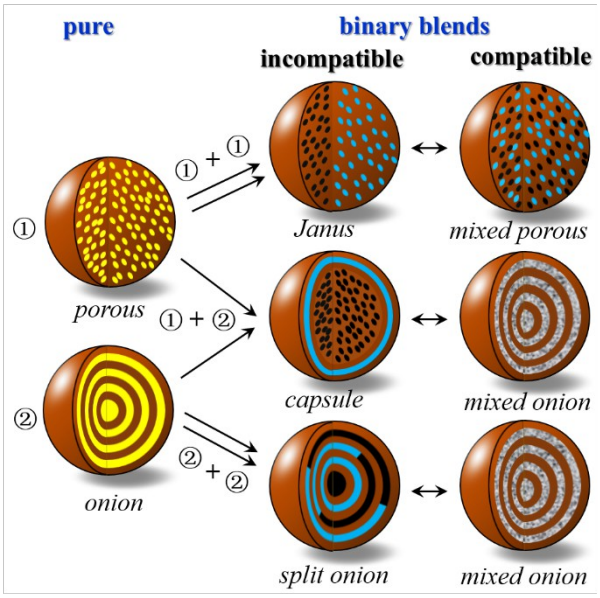

Scheme 1. Schematic illustrations of the cooperative self-assembly strategies of binary diblock copolymer blends for novel morphologies. The combination procedure from “pure” to “binary blend” indicates a blend of two different diblock copolymers. The arrows between different binary micelles indicate a possible transition by modifying the incompatibility of blocks. Brown domains denote pure hydrophilic blocks; yellow, blue and dark domains denote pure hydrophobic blocks; white-dark domains denote hydrophobic block blends.

3.3 Cooperative Self-Assembly of Ternary AB/AC/AD Systems

To further expand the number of morphologies, blending of ternary AB/AC/AD diblock copolymers leads to multicompartment micelles with more complex compartment distributions in the core or shell[18,50]. Based on the assembly pathways in the binary system above, the central challenge of the ternary system lies in confining multiple phases that spontaneously blend or separate under different incompatibilities, which is driven by unfavorable mixing enthalpy[14]. In AB/AC/AD co-assembled blends, we emphasize two major aspects, i.e., tuning multiple hydrophobic phases in either the shell or core region of the microcapsule micelles obtained above by the additional D block. As depicted in Figure 7, nanoassemblies with mixed shell and pure core domains are observed if the segregation degrees of AB and AC are much larger than AD (a_{AB} = a_{AC} = 60 and a_{AD} = 37.04). These morphologies can be obtained from a one-step co-assembly of the ternary blends driven by the gap of the stretching forces between AB/AC and AD. The incompatibility of B and C drives demixing of the shell from multipatch for weak repulsion (a_{BC} = 25) to complete Janus separation for strong repulsion (a_{BC} = 45). Two possible distribution patterns are obtained for the Janus separation of the cylindrical micelle shell. The shell characteristics of the

multicompartment micelles can be controlled by modifying the solvophobic interaction of the two hydrophobic blocks in the shell. The ϕ_{AB} : ϕ_{AC} : ϕ_{AD} values for the spherical and cylindrical micelles in Figure 7 are 6.5% : 6.5% : 7% and 8.75% : 8.75% : 12.5%, respectively, leading to complete AB/AC shells and kinetically trapped AD cores. More shell structures with different thickness or coverage are available by controlling the copolymer concentration or architectures in the ternary system.

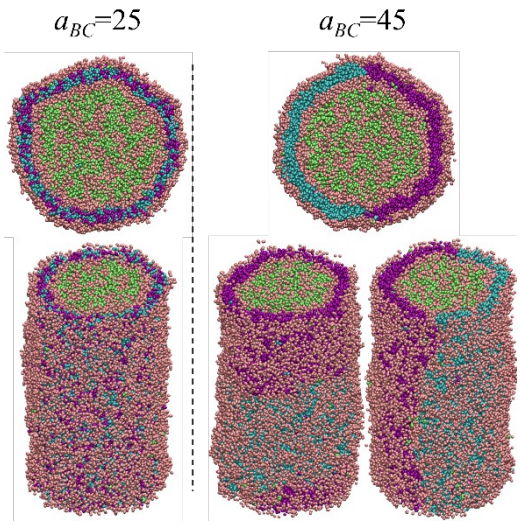

Figure 7. Morphologies of the spherical (cross sections, ϕ_{AB} : ϕ_{AC} : ϕ_{AD} = 6.5% : 6.5% : 7%) and cylindrical (ϕ_{AB} : ϕ_{AC} : ϕ_{AD} = 8.75% : 8.75% : 12.5%) micelles with mixed shells (AB/AC) and pure cores (AD) (a_{AB} = a_{AC} = 60, a_{AD} = 37.04). Color scheme: A-pink, B-cyan, C-purple, D-green.

For nanoassemblies with pure shell and mixed core domains (Figure 8), morphologies were obtained from a two-step co-assembly process. First, interaction parameters of a_{AB} = 60, a_{AC} = a_{AD} = 37.04 and a_{BC} = a_{BD} = 45 were implemented to make sure that AC/AD can be kinetically trapped and separated by AB. The ϕ_{AB} : ϕ_{AC} : ϕ_{AD} values are 13% : 3.5% : 3.5% and 17.5% : 6.25% : 6.25% for the spherical and cylindrical micelles, respectively, leading to complete AB shells. Second, co-assembly of the AC/AD blend at the core was initiated by

adopting different segregation degrees or repulsions of the two copolymers. At a_{AC} = a_{AD} = 37.04, the incompatibility of C and D drives demixing of the core from multipatch for weak repulsion (a_{CD} = 25) to complete Janus separation for strong repulsion (a_{CD} = 45). If the segregation degree of AC is increased (e.g., a_{AC} = 60, a_{AD} = 37.04), onion-like core morphology is obtained at a_{CD} = 25 (compatible C and D), and capsule-like core morphology is obtained at a_{CD} = 45 (incompatible C and D). If AC and AD have large segregation degrees (a_{AC} = a_{AD} = 60), better-ordered onion-like core morphology with mixed or split AC/AD compartments are observed at a_{CD} = 25 (compatible C and D) and a_{CD} = 45 (incompatible C and D), respectively. These self-assemblies of the AC/AD blend within the confined spherical or tubular spaces are seen to be consistent with those without the confining wall. Thus, our binary structures are transferable to ternary microcapsules preserving self-repulsive and block compatibility dependent cooperative self-assembly patterns.

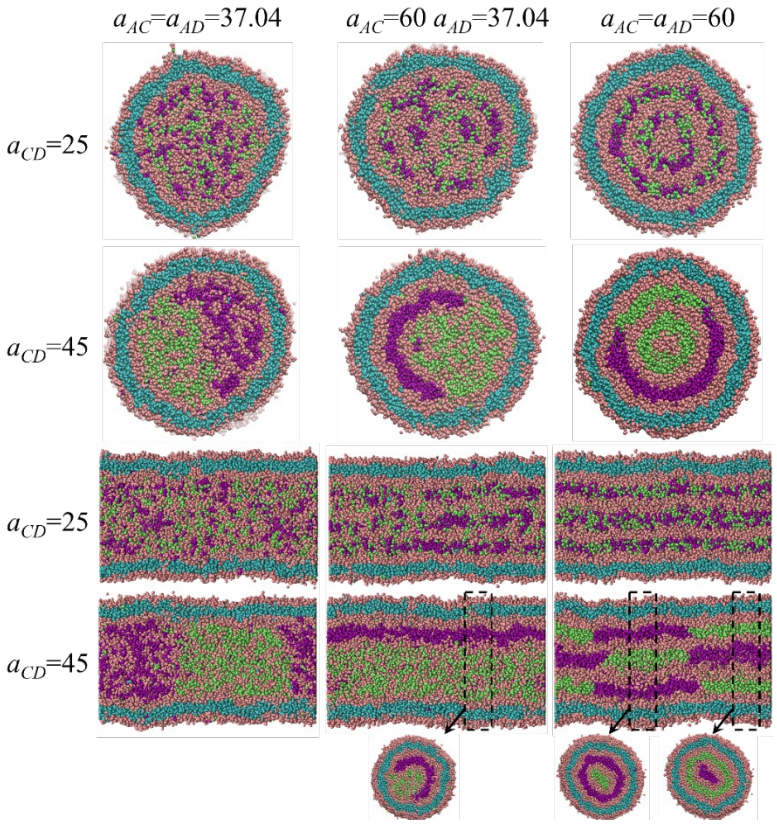

Figure 8. Morphologies of the spherical (cross sections, ϕ_{AB} : ϕ_{AC} : ϕ_{AD} = 13% : 3.5% : 3.5%) and cylindrical (cross sections, ϕ_{AB} : ϕ_{AC} : ϕ_{AD} = 17.5% : 6.25% : 6.25%) micelles with pure shells (AB) and mixed cores (AC/AD) (a_{AB} = 60). Color scheme as in Figure 7.

Since the local composition and structure of the ternary microcapsule can be tuned by changing the interactions of the blocks, we now explore a manipulation of the microcapsule from the "mixed shell/pure core" structure to the "pure shell/mixed core" structure (Figure 9). During this transition, only the repulsive forces between different hydrophobic blocks are modified, while the segregation degrees of copolymers remain unchanged at a_{AB} = 60, a_{AC} = 45 and a_{AD} = 37.04. For a "pure shell/mixed core" structure like (a1) or (b1) (a_{BC} = a_{BD} = 45, a_{CD} = 25), if the repulsion between C and D is increased (a_{BC} = a_{BD} = a_{CD} = 45), the AC/AD blend will be split and form a "layer-by layer" structure like (a3) or (b3) due to the gap of the segregation degrees between AC and AD. Based on this structure, if the repulsion between B and C is decreased (a_{BC} = 25, a_{BD} = a_{CD} = 45), the initial-split AB and AC layers will blend with each other and form a "mixed shell/pure core" structure like (a5) or (b5). (a2)/(b2) and (a4)/(b4) show the intermediate states of the two processes. Also, the two processes can be reversed if the interactions between the hydrophobic blocks are modified in another direction. The ϕ_{AB} : ϕ_{AC} : ϕ_{AD} values are 13% : 5.7% : 1.3% and 17.5% : 10% : 2.5% for the spherical and cylindrical micelles, respectively, leading to three complete, separate layers in (a3) and (b3). The above strategy exhibits great potential in tuning the surficial or inner property of microcapsule micelles.

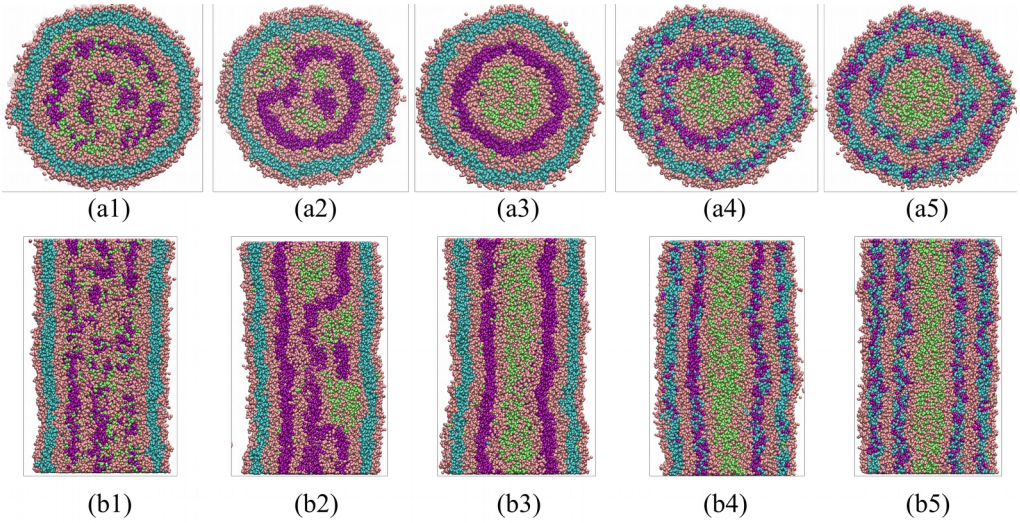

Figure 9. Manipulation of the structural transitions of spherical (cross sections, ϕ_{AB} : ϕ_{AC} : ϕ_{AD} = 13% : 5.7% : 1.3%) and cylindrical (cross sections, ϕ_{AB} : ϕ_{AC} : ϕ_{AD} = 17.5% : 10% : 2.5%) micelles from the "pure shell/mixed core" state (a1, b1) to the "mixed shell/pure core" state (a5, b5) by adjusting the interactions between hydrophobic blocks. (a2 ~ a4) and (b2 ~ b4) indicate the intermediate states. Color scheme as in Figure 7.

The formation of ternary multicompartment micelles with specific local structures is illustrated in Scheme 2. Two co-assembly pathways combining a pure porous micelle and a pure onion-like micelle, relating to weak and strong segregation degrees of copolymers, is presented. In the ternary system, the combination of two porous micelles and an onion-like micelle will lead to morphologies such as "pure shell/Janus core", "pure shell/mixed core", "ternary mixed onion", and "mixed shell/pure core"; the combination of a porous micelle and two onion-like micelles will lead to morphologies such as "pure shell/split core", "pure shell/mixed onion core", "split shell/pure core", and "mixed onion shell/pure core". The co-assembly mechanism of the ternary blends is basically consistent with that in the binary blends, and we are able to manipulate more specifically the local structure and composition

of the shell or core regions in ternary micelles through the third component. Moreover, it is noteworthy that some of these morphologies are obtained from a two-step simulation, during which an alteration of block interactions (intra- or inter-) are needed. We expect that the experimental preparation of such nanostructures may be accomplished by modifying solution parameters or environment stimuli. In combination with Scheme 1, we present a systematic understanding for the construction of multicompartment micelles with large compositional and geometrical complexity through the co-assembly of diblock copolymer blends. These schemes can be applied to both spherical and cylindrical micelles according to our simulations.

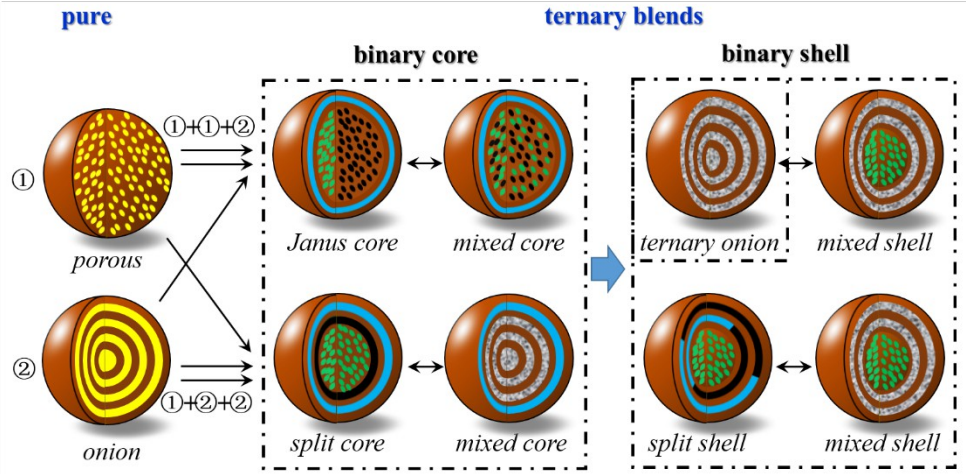

Scheme 2. Schematic illustrations of the cooperative self-assembly strategy of ternary diblock copolymer blends for novel morphologies. The combination procedure from “pure” to “ternary blend” indicates a blend of three different diblock copolymers. The arrows between different ternary micelles indicate a possible transition by modifying the incompatibility of blocks. Brown domains denote pure hydrophilic blocks; yellow, blue, dark and green domains denote pure hydrophobic blocks; white-dark domains denote hydrophobic block blends.

4 Conclusions

In this paper, a strategy combining the advantages of diblock copolymer blending and incompatibility-induced phase separation is proposed to prepare multicompartment spherical and cylindrical micelles from AB, AB/AC and AB/AC/AD systems. AB self-assembled micelles exhibit sponge-like compartments and well-ordered onion-like compartments with weak and strong stretching degrees of AB, respectively. In AB/AC blends, the formation of the typical compartmentalized micelles including morphologies of sponge, Janus, capsule, onion, etc. was investigated, and it was suggested that the relative stretching or incompatibility of AB and AC were involved in the morphologies of the co-assembled micelles. The formation of microcapsule micelles with separate AB shell and AC core was explored and mechanism was attributed to the large stretching difference of the two polymers. Further, in AB/AC/AD blends, we demonstrate the preparation of multicompartment micelles with more intricate structures and morphologies at the core or shell by modifying the interaction parameters affecting the relative stretching or incompatibility of copolymers. In particular, a method involving the manipulation of block repulsions was revealed for regulating the shell and core composition or morphology of the ternary multicompartment micelle. Our results demonstrate an efficient methodology for the preparation of multicompartment micelles with ingenious morphologies through the co-assembly of diblock copolymer blends, and some of which, such as the structural adjustable microcapsule micelles, are expected to have potential application.

Acknowledgments

This research was financially supported by the Fundamental Research Funds for the Central Universities (14CX02221A, 16CX06023A and 16CX05017A), and the Applied Fundamental

Research Foundation of Qingdao Independent Innovation Plan (15-9-1-46-jch and 16-5-1-90-jch). The authors also acknowledge support from the China Scholarship Council.

References

1 Löbling, T. I.; Borisov, O.; Haataja, J. S.; Ikkala, O.; Gröschel, A. H.; Müller, A. H. *Nature Communications* 2016, **7**.

2 Li, L.; Matsunaga, K.; Zhu, J.; Higuchi, T.; Yabu, H.; Shimomura, M.; Jinnai, H.; Hayward, R. C.; Russell, T. P. *Macromolecules* 2010, **43**, 7807-7812.

3 Jang, S. G.; Audus, D. J.; Klinger, D.; Krogstad, D. V.; Kim, B. J.; Cameron, A.; Kim, S.-W.; Delaney, K. T.; Hur, S.-M.; Killops, K. L. *Journal of the American Chemical Society* 2013, **135**, 6649-6657.

4 Jeon, S. J.; Yi, G. R.; Yang, S. M. *Advanced Materials* 2008, **20**, 4103-4108.

5 Paradiso, S. P.; Delaney, K. T.; García-Cervera, C. J.; Ceniceros, H. D.; Fredrickson, G. H. *ACS Macro Letters* 2014, **3**, 16-20.

6 Zhu, X.; Liu, M. *Langmuir* 2011, **27**, 12844-12850.

7 Wang, X.; Guerin, G.; Wang, H.; Wang, Y.; Manners, I.; Winnik, M. A. *Science* 2007, **317**, 644-647.

8 Li, Z.; Kesselman, E.; Talmon, Y.; Hillmyer, M. A.; Lodge, T. P. *Science* 2004, **306**, 98-101.

9 Cai, C.; Wang, L.; Lin, J.; Zhang, X. *Langmuir* 2012, **28**, 4515-4524.

10 Jiang, T.; Wang, L.; Lin, S.; Lin, J.; Li, Y. *Langmuir* 2011, **27**, 6440-6448.

11 Luo, Z.; Jiang, J. *Journal of Controlled Release* 2012, **162**, 185-193.

12 Cheng, L.; Lin, X.; Wang, F.; Liu, B.; Zhou, J.; Li, J.; Li, W. *Macromolecules* 2013, **46**, 8644-8648.

13 Li, Z.; Wang, P.; Yan, Y.; Wang, R.; Zhang, J.; Dai, C.; Hu, S. *The Journal of Physical Chemistry Letters* 2013, **4**, 3962-3966.

14 Mai, Y.; Eisenberg, A. *Chemical Society Reviews* 2012, **41**, 5969-5985.

15 Zhang, L.; Eisenberg, A. *Journal of the American Chemical Society* 1996, **118**, 3168-3181.

16 Zhang, L.; Eisenberg, A. *Polymers for Advanced Technologies* 1998, **9**, 677-699.

17 Shi, P.; Qu, Y.; Liu, C.; Khan, H.; Sun, P.; Zhang, W. *ACS Macro Letters* 2015, **5**, 88-93.

18 Moughton, A. O.; Hillmyer, M. A.; Lodge, T. P. *Macromolecules* 2012, **45**, 2-19.

19 Gröschel, A. H.; Schacher, F. H.; Schmalz, H.; Borisov, O. V.; Zhulina, E. B.; Walther, A.; Müller, A. H. *Nature Communications* 2012, **3**, 710.

20 Du, J.; O'Reilly, R. K. *Chemical Society Reviews* 2011, **40**, 2402-2416.

21 Yan, N.; Sheng, Y.; Liu, H.; Zhu, Y.; Jiang, W. *Langmuir* 2015, **31**, 1660-1669.

22 Hofman, A. H.; ten Brinke, G.; Loos, K. *Polymer* 2016, **107**, 343-356.

23 Cai, C.; Li, Y.; Lin, J.; Wang, L.; Lin, S.; Wang, X. S.; Jiang, T. *Angewandte Chemie International Edition* 2013, **52**, 7732-7736.

24 Cambridge, G.; Gonzalez-Alvarez, M. J.; Guerin, G.; Manners, I.; Winnik, M. A. *Macromolecules* 2015, **48**, 707-716.

25 Cai, C.; Lin, J.; Chen, T.; Wang, X.-S.; Lin, S. *Chemical Communications* 2009, 2709-2711.

26 Kamps, A. C.; Fryd, M.; Park, S.-J. *ACS Nano* 2012, **6**, 2844-2852.

27 Chen, Y.; Zhang, K.; Wang, X.; Zhang, F.; Zhu, J.; Mays, J. W.; Wooley, K. L.; Pochan, D. J. *Macromolecules* 2015, **48**, 5621-5631.

28 Zhu, J.; Zhang, S.; Zhang, K.; Wang, X.; Mays, J. W.; Wooley, K. L.; Pochan, D. J. *Nature Communications* 2013, **4**.

29 Wright, D. B.; Patterson, J. P.; Gianneschi, N. C.; Chassenieux, C.; Colombani, O.; O'Reilly, R. K. *Polymer Chemistry* 2016, **7**, 1577-1583.

30 Wright, D. B.; Patterson, J. P.; Pitto-Barry, A.; Lu, A.; Kirby, N.; Gianneschi, N. C.; Chassenieux, C.; Colombani, O.; O'Reilly, R. K. *Macromolecules* 2015, **48**, 6516-6522.

31 Palanisamy, A.; Guo, Q. *The Journal of Physical Chemistry B* 2014, **118**, 12796-12803.

32 Christian, D. A.; Tian, A.; Ellenbroek, W. G.; Levental, I.; Rajagopal, K.; Janmey, P. A.; Liu, A. J.; Baumgart, T.; Discher, D. E. *Nature Materials* 2009, **8**, 843-849.

33 Han, S. H.; Pryamitsyn, V.; Bae, D.; Kwak, J.; Ganesan, V.; Kim, J. K. *ACS Nano* 2012, **6**, 7966-7972.

34 Vyhnalkova, R.; Müller, A. H.; Eisenberg, A. *Langmuir* 2014, **30**, 13152-13163.

35 Vyhnalkova, R.; Müller, A. H.; Eisenberg, A. *Langmuir* 2014, **30**, 5031-5040.

36 Srinivas, G.; Pitera, J. W. *Nano Letters* 2008, **8**, 611-618.

37 Zhu, J.; Hayward, R. C. *Macromolecules* 2008, **41**, 7794-7797.

38 Gao, C.; Wu, J.; Zhou, H.; Qu, Y.; Li, B.; Zhang, W. *Macromolecules* 2016, **49**, 4490-4500.

39 Sliozberg, Y.; Strawhecker, K.; Andzelm, J.; Lenhart, J. *Soft Matter* 2011, **7**, 7539-7551.

40 Walther, A.; Müller, A. H. *Soft Matter* 2008, **4**, 663-668.

41 Pochan, D. J.; Chen, Z.; Cui, H.; Hales, K.; Qi, K.; Wooley, K. L. *Science* 2004, **306**, 94-97.

42 Cui, H.; Chen, Z.; Zhong, S.; Wooley, K. L.; Pochan, D. J. *Science* 2007, **317**, 647-650.

43 Zheng, R.; Liu, G.; Yan, X. *Journal of the American Chemical Society* 2005, **127**, 15358-15359.

44 Habersberger, B. M.; Gillard, T. M.; Hickey, R. J.; Lodge, T. P.; Bates, F. S. *ACS Macro*

Letters 2014, **3**, 1041-1045.

45 Asai, Y.; Yamada, K.; Yamada, M.; Takano, A.; Matsushita, Y. *ACS Macro Letters* 2014, **3**, 166-169.

46 Liu, M.; Qiang, Y.; Li, W.; Qiu, F.; Shi, A.-C. *ACS Macro Letters* 2016, **5**, 1167-1171.

47 Gohy, J.-F.; Lefèvre, N.; D'haese, C.; Hoeppener, S.; Schubert, U. S.; Kostov, G.; Améduri, B. *Polymer Chemistry* 2011, **2**, 328-332.

48 Luo, L.; Eisenberg, A. *Angewandte Chemie International Edition* 2002, **41**, 1001-1004.

49 Discher, D. E.; Ahmed, F. *Annu. Rev. Biomed. Eng.* 2006, **8**, 323-341.

50 Gröschel, A. H.; Müller, A. H. *Nanoscale* 2015, **7**, 11841-11876.

51 Holder, S. J.; Sommerdijk, N. A. *Polymer Chemistry* 2011, **2**, 1018-1028.

52 Stuart, M. A. C.; Huck, W. T.; Genzer, J.; Müller, M.; Ober, C.; Stamm, M.; Sukhorukov, G. B.; Szleifer, I.; Tsukruk, V. V.; Urban, M. *Nature Materials* 2010, **9**, 101-113.

53 Singh, N. K.; Lee, D. S. *Journal of Controlled Release* 2014, **193**, 214-227.

54 Groot, R. D.; Warren, P. B. *The Journal of Chemical Physics* 1997, **107**, 4423-4435.

55 Luo, Z.; Li, Y.; Wang, B.; Jiang, J. *Macromolecules* 2016, **49**, 6084-6094.

56 Spaeth, J. R.; Kevrekidis, I. G.; Panagiotopoulos, A. Z. *The Journal of Chemical Physics* 2011, **135**, 184903.

57 Spaeth, J. R.; Kevrekidis, I. G.; Panagiotopoulos, A. Z. *The Journal of Chemical Physics* 2011, **134**, 164902.

58 Plimpton, S. *Journal of Computational Physics* 1995, **117**, 1-19.

59 Karunakaran, M.; Nunes, S. P.; Qiu, X.; Yu, H.; Peinemann, K.-V. *Journal of Membrane Science* 2014, **453**, 471-477.

60 Yang, Y.-W.; Sun, Y.-L.; Song, N. *Accounts of Chemical Research* 2014, **47**, 1950-1960.

For Table of Contents use only:

Controllable multicompartment morphologies from cooperative self-assembly of copolymer-copolymer blends[b†]

Zhikun Wang[a,b], Shuangqing Sun[a,c], Chunling Li[a,c], Songqing Hu[a,c*], Roland Faller[b*]

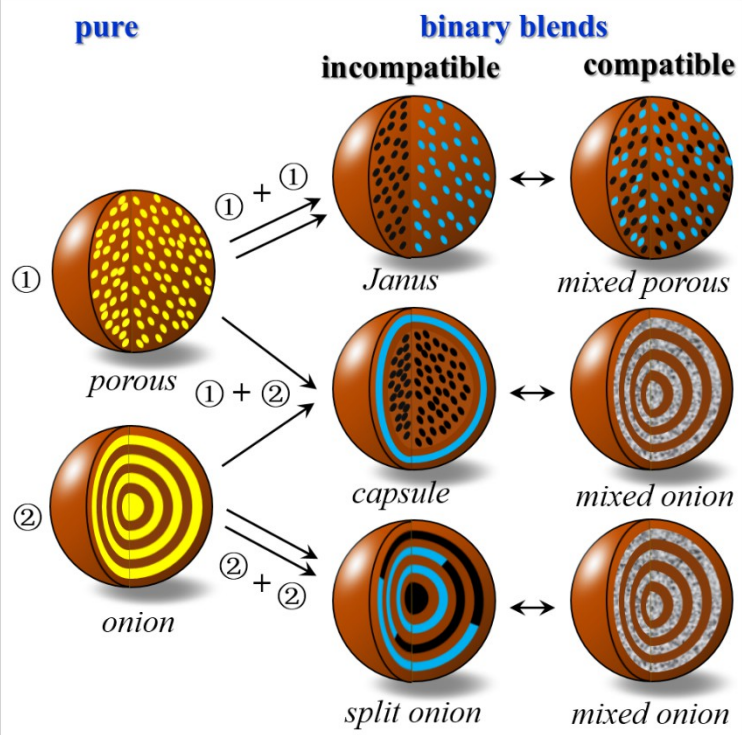

b† Electronic Supplementary Information (ESI) available. See DOI: XXXXXXXXX.

aa College of Science, China University of Petroleum (East China), 266580 Qingdao, Shandong, China. E-mail: songqinghu@upc.edu.cn

bb Department of Chemical Engineering, UC Davis, 95616 Davis, California, USA. E-mail: rfaller@ucdavis.edu

cc Key Laboratory of New Energy Physics & Materials Science in Universities of Shandong, China University of Petroleum (East China), 266580 Qingdao, Shandong, China.